frontiers | Frontiers in Communications and Networks

TYPE Original Research
PUBLISHED 05 May 2023
DOI 10.3389/frcmn.2023.1184911



OPEN ACCESS

EDITED BY
Nikolaos Nomikos,
National and Kapodistrian University of Athens, Greece

REVIEWED BY
Kapila Palitharathna,
Sri Lanka Technological Campus, Sri Lanka
Prabhat Kumar Upadhyay,
Indian Institute of Technology Indore, India
Sotiris Tegos,
Aristotle University of Thessaloniki, Greece

*CORRESPONDENCE
Yalçın Ata,
ylcnata@gmail.com

RECEIVED 12 March 2023
ACCEPTED 17 April 2023
PUBLISHED 05 May 2023

CITATION
Ata Y and Alouini M-S (2023), Outage probability analysis of maritime FSO links. *Front. Comms. Net* 4:1184911. doi: 10.3389/frcmn.2023.1184911



# Outage probability analysis of maritime FSO links

Yalçın Ata[1]* and Mohamed-Slim Alouini[2]

[1]Department of Electrical and Electronics Engineering, OSTIM Technical University, Ankara, Türkiye, [2]Computer Electrical and Mathematical Sciences and Engineering (CEMSE) Division, King Abdullah University of Science and Technology (KAUST), Thuwal, Saudi Arabia

In this paper, the outage performance of the maritime free-space optical (FSO) communication system is analyzed, and a new maritime FSO link configuration is presented. The channel model for maritime FSO link includes the combined effect of turbulence, pointing error, angle-of-arrival (AOA) fluctuations, and attenuation. While the maritime turbulence channel is modeled by lognormal distribution, pointing error and AOA fluctuations are assumed to be Beckmann and Rayleigh distributed, respectively. The turbulence power spectrum is considered to present the Kolmogorov characteristics, and the Rytov variance of a propagating Gaussian beam in maritime environment is obtained. The probability density function (PDF), cumulative distribution function (CDF), and outage probability of the maritime communication channel are obtained analytically. The outage performance of a maritime communication link is given depending on various parameters of the maritime environment, the Gaussian beam, and the (FSO) communication system.

KEYWORDS

**free-space optics, optical wireless communication, maritime communication, outage probability, maritime networks**

## 1 Introduction

Not only terrestrial links but also maritime and underwater communication links have been widely investigated in recent years to meet growing demands, such as high data rate, large bandwidth, secure and licence-free communication, and noise immunity, in many industrial applications. Due to its high potential in terms of providing communication services for various types of links, including ship-to-shore, ship-to-underwater sensor networks, ship-to-satellite, and ship-to-ship communications, maritime-based free-space optical (FSO) communication is a prominent candidate to meet the challenging requirements of these communication systems. The trend is heading toward wireless communication systems in which acoustic and radio frequency (RF)-based communication systems are replaced by their optical spectrum-based counterparts. The evolution of maritime communication systems, marine technologies, various applications and their integrations, autonomous networks, and implementation challenges have been comprehensively evaluated in the studies by Kidston and Kunz (2008); Zolich et al. (2019); Alqurashi et al. (2022). The performance of a maritime communication network capable of wideband video communication was analyzed considering energy efficiency (Yang and Shen, 2014). In a study by Jo and Shim (2019), a long-time evolution (LTE) maritime project that aims to develop a maritime communication network structure providing several Mbit/s data rate up to 100 km coverage area was introduced, and a ship-to-shore data communication link was experimentally shown to be an alternative of maritime communication. The architecture of a comprehensive maritime communication network, including space, air,

shore, surface, and underwater, was proposed by Guan et al. (2021), and path loss with the optimum height of base stations for different scenarios was presented.

To characterize the effect of maritime environment on the behavior of optical wireless communication systems, the variation of optical signal intensity's attenuation in maritime fog environments was studied experimentally, and distribution functions were obtained (Awan et al., 2008). The availability of a hybrid network of an RF/FSO link was examined by Gregory and Badri-Hoeher (2011), and both optical transmission and correlation were obtained for a 14-km FSO link considering environment parameters. An experimental work was conducted for a 7.2-km propagation path to develop a model for performance evaluation of FSO communication link in near-surface marine environment that is a base for ship-to-ship and ship-to-shore FSO communication links (Gadwal and Hammel, 2006). The demonstration of a 1,550-nm FSO communication link in maritime environment having a data rate of up to 5 Mbits/s over a distance of 2 km was presented by Rabinovich et al. (2005), and an atmospheric channel was modeled by gamma–gamma distribution. Then, experimental and theoretical results for the link budget were compared. Performance analysis of an FSO communication system in terms of received signal strength was performed experimentally for an approximately 3-km FSO link under specific weather conditions (especially rain) (Lionis et al., 2020). The bit-error-rate (BER) of an FSO communication system operating in maritime environment was measured for weak and moderate turbulence conditions, and the obtained results were compared with the results obtained theoretically from lognormal and gamma–Gamma distributed channel models (Kampouraki et al., 2014). Cvijetic and Li (2017) studied the BER performance of both terrestrial and maritime FSO communication systems in uplink and downlink directions. They showed that an improvement in the BER performance can be obtained by applying adaptive optics (AO) compensation. In another study (Juarez et al., 2010), the benefit of AO compensation on the performance of FSO communication systems in the maritime environment was again shown, and the variation of optical power was examined for a ship-to-shore link operating at 2.5 Gbits/s and 2–22 km link lengths. Data transmission and packets being lost for an FSO communication system operating in the maritime environment were analyzed for 5–16 km link lengths, and it was shown that the number of packets being lost increases sharply when the packet size exceeds 1 millisecond (Sluz et al., 2010).

Kim et al. (2016) examined the BER performance of a maritime-based visible light communication (VLC) system modeled by gamma–gamma distribution, and it was shown that the maximal ratio combining (MRC) technique presents superiority in terms of link quality. The BER performance of an FSO link using on–off keying (OOK) modulation scheme in weak non-Kolmogorov maritime turbulent medium was reflected numerically by Cheng et al. (2015). Recently, the BER performance of an FSO communication system using a differential phase shift keying (DPSK) modulation scheme in the maritime environment has been investigated by taking into account only the turbulence effect (assuming that turbulence presents non-Kolmogorov characteristics) that is modeled by lognormal distribution (Qiao et al., 2021).

Although a certain number of studies have been devoted to characterizing the performance of FSO communication systems in the maritime environment, there are still many different scenarios, applications, and parameters that remain to be studied to provide more reliable communication and meet the growing requirements. To take the existing works one step further, we propose a new model for outage performance of maritime FSO links, including a combined effect of maritime turbulence, pointing error, angle-of-arrival (AOA) fluctuations, and attenuation. In the present work, the maritime turbulence is assumed to present the Kolmogorov spectrum characteristics, and the maritime turbulent channel is modeled by lognormal distribution. The pointing error is modeled by the Beckmann distribution, which allows the utilization of asymmetric displacements resulting from different misalignments in both vertical and horizontal directions. AOA fluctuations are assumed to follow Rayleigh distribution. We can summarize our contribution as follows:

- To make our analysis as comprehensive and realistic as possible, the effects of maritime turbulence, attenuation, pointing error, and AOA fluctuations are combined. To the best of our knowledge, this is the first time that the performance analysis for a maritime FSO communication system involving so many phenomena and superposing their impacts is carried out in the maritime environment.
- The maritime turbulent channel is assumed to follow lognormal distribution. Pointing error is modeled by the Beckmann distribution, which permits asymmetric beam deviation in horizontal and vertical directions. AOA fluctuations are selected to be Rayleigh distributed.
- Maritime turbulence is taken into account over a wide range, including weak, moderate, and strong turbulence conditions. Thus, the analysis of the performance of FSO links becomes possible for a wide range of turbulence regimes in the maritime environment.
- According to the extended Rytov theory, the Rytov variances of both plane wave and Gaussian beam are used to find the intensity fluctuations, namely, the scintillation index, in the maritime turbulent environment. To perform this, the analytical form of the Rytov variance for the Gaussian beam is obtained considering that the maritime turbulence spectrum is in Kolmogorov statistics.
- Closed-form expressions for channel probability density function (PDF) and cumulative distribution function (CDF) are derived.
- Outage performance of FSO links in the maritime environment is obtained by deriving the outage probability in an analytical form.
- We also provide a comparison of outage performances of maritime and terrestrial FSO links.

Due to involving various applications from different industries, the conventional communication links between maritime–underwater, maritime–maritime, maritime–aerial, and maritime–satellite platforms evolve into FSO links. While limited fourth-generation (4G) systems are gradually replaced by fifth-generation (5G) and sixth-generation (6G) technologies, increasing demands for high-speed data rates; large bandwidth;

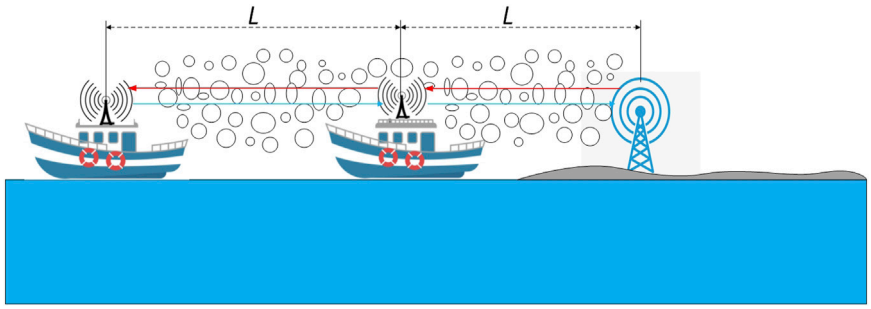


FIGURE 1
System model.

and reliable, secure, and noise-immune communication make it necessary to analyze the maritime-based communication system more comprehensively and precisely. Our motivation in this deeply analyzed study is to model maritime FSO communication links more accurately by taking into account as many involved phenomena as possible and reflect the performance of maritime FSO links depending on the various relevant aspects.

## 2 System and channel models

The system model is given in Figure 1. Our proposed model is quite comprehensive in terms of combining the effects of pointing error, AOA fluctuations, attenuation, and turbulence. Possible scenarios for maritime-based communications are horizontal ship-to-ship and ship-to-shore FSO links. The link length is denoted by $L$. The performance of horizontal maritime FSO links is analyzed in terms of outage probability. The maritime turbulence is considered to be the Kolmogorov spectrum, and the channel is modeled by lognormal distribution. To describe the intensity fluctuations resulting from a wide range of turbulence regimes in the maritime environment, the Rytov variance of a propagating Gaussian beam is obtained, and it is given as an input for calculation of the scintillation index. The beam displacements are modeled by the well-known Beckmann distribution that does not require the same deviations in vertical and horizontal directions. The Rayleigh distribution is used to represent the AOA fluctuations.

The combined channel state is expressed by

$$h = h_{al} h_{at} h_{pl} h_{af}, \tag{1}$$

where $h_{al}$, $h_{at}$, $h_{pl}$, and $h_{af}$ represent the attenuation, maritime turbulence, pointing error, and AOA fluctuations, respectively, and their details are given in the following subsections.

### 2.1 Attenuation

According to the Beer–Lambert law, the attenuation in the maritime environment can be expressed depending on the absorption and scattering as

$$h_{al} = \exp(-\alpha L), \tag{2}$$

where $\alpha$ is the attenuation coefficient, and $L$ is the length of the maritime FSO link. The attenuation coefficient $\alpha$ is calculated by using the visibility parameter as (Naboulsi et al., 2004)

$$\alpha = 3.912(\lambda/550)^{-q}/V, \tag{3}$$

where $V$ denotes the visibility (in km), $\lambda$ is the optical beam wavelength (in nm), and the parameter $q$ is defined in the Kim model as (Naboulsi et al., 2004)

$$q = \begin{cases} 1.6, & V > 50\ \text{Km} \\ 1.3, & 6\ \text{Km} < V < 50\ \text{Km} \\ 0.16V + 0.34, & 1\ \text{Km} < V < 6\ \text{Km} \\ V - 0.5, & 0.5\ \text{Km} < V < 1\ \text{Km} \\ 0, & V < 0.5\ \text{Km} \end{cases}. \tag{4}$$

### 2.2 Maritime turbulence

The PDF of the maritime turbulence channel that is modeled by lognormal distribution is given by (Andrews and Phillips, 2005)

$$f_{h_{at}}(h_{at}) = \frac{1}{h_{at}\sqrt{2\pi\sigma_l^2}} \exp\left\{-\left[\frac{\ln(h_{at}) + 0.5\sigma_l^2}{\sqrt{2\sigma_l^2}}\right]^2\right\}, \tag{5}$$

where $h_{at} > 0$ is the channel state of maritime turbulence, $\sigma_l^2 = \ln(\sigma_I^2 + 1)$ is the log-irradiance variance; $\sigma_I^2$ is the scintillation index, and it can be calculated by (Andrews and Phillips, 2005)

$$\sigma_I^2 = \exp\left[\sigma_{lnX}^2(D_G) + \sigma_{lnY}^2(D_G)\right] - 1, \tag{6}$$

where $D_G$ is the diameter of the receiver aperture, $\sigma_{lnX}^2$ is the large-scale log variance, and $\sigma_{lnY}^2$ is the small-scale log variance.

$\sigma_{lnX}^2$ and $\sigma_{lnY}^2$ are found (Andrews and Phillips, 2005) as

$$\sigma_{lnX}^2 = \frac{0.49\left(\frac{\Omega_G - \Lambda_1}{\Omega_G + \Lambda_1}\right)^2 \sigma_B^2}{\left[1 + 0.56(1 + \Theta_1)\sigma_B^{12/5} + \frac{0.4(2 - \bar{\Theta}_1)(\sigma_B/\sigma_R)^{12/7}}{(\Omega_G + \Lambda_1)\left(1/3 - 0.5\bar{\Theta}_1 + 0.2\bar{\Theta}_1^2\right)^{6/7}}\right]^{7/6}}, \tag{7}$$

$$\sigma_{lnY}^2 = \frac{0.51\sigma_B^2\left(1 + 0.69\sigma_B^{12/5}\right)^{-5/6}}{1 + \left[1.20(\sigma_R/\sigma_B)^{12/5} + 0.83\sigma_R^{12/5}\right]/(\Omega_G + \Lambda_1)}, \tag{8}$$

where $\Omega_G = 2L/(kW_G^2)$ is the non-dimensional Fresnel parameter, $k = 2\pi/\lambda$ is the wave number, $\lambda$ is the wavelength of the optical beam, $W_G = D_G/\sqrt{8}$ is the radius of the Gaussian lens, $\Lambda_0 = 2L/(kW_0^2)$, $W_0$ is the beam radius, $\Lambda_1 = \Lambda_0/(\Lambda_0^2 + \Theta_0^2)$ is the Fresnel ratio of the Gaussian beam at the receiver, $F_0$ is the phase front radius of curvature, $\Theta_0 = 1 - L/F_0$ and $\Theta_1 = \Theta_0/(\Lambda_0^2 + \Theta_0^2)$ are the beam curvature parameters at the transmitter and receiver, $\bar{\Theta}_1 = 1 - \Theta_1$ is the complementary parameter. The terms $\sigma_R^2$ and $\sigma_B^2$ are the Rytov variances of plane and Gaussian beam waves in the maritime turbulent environment.

The Rytov variance of the plane wave $\sigma_R^2$ is expressed (Grayshan et al., 2008) by

$$\sigma_R^2 = 4.75C_n^2k^{7/6}L^{11/6}\left\{\left(1+\frac{1}{Q_H^2}\right)^{11/12}\left[\sin\left(\frac{11}{6}\arctan Q_H\right) - \frac{0.051\sin\left(\frac{4}{3}\arctan Q_H\right)}{\left(1+Q_H^2\right)^{1/4}} + \frac{3.052\sin\left(\frac{5}{4}\arctan Q_H\right)}{\left(1+Q_H^2\right)^{7/24}}\right] - 5.581Q_H^{-5/6}\right\}, \tag{9}$$

where $C_n^2$ is the turbulence structure constant, $Q_H = Lk_H^2/k$, $\kappa_H = 3.41/l_0$, $l_0$ is the inner scale length of maritime turbulence.

Proposition 1: The Rytov variance of the Gaussian beam $\sigma_B^2$ is obtained in this study by

$$\begin{aligned}\sigma_B^2 = \frac{0.132\pi^2k^2C_n^2L}{\kappa_H^{5/3}}\{&\Gamma(-5/6)_2F_1(-5/6,1/2;3/2;-Q_l)\\ &-0.061\Gamma(-1/3)_2F_1(-1/3,1/2;3/2;-Q_l)\\ &+2.836\Gamma(-1/4)_2F_1(-1/4,1/2;3/2;-Q_l)\\ &-\frac{6\Gamma\left(-\frac{5}{6}\right)}{11Z_2}\left[Z_1^{11/6}\cos\left(\frac{11\Psi_1}{6}-\Psi_2\right)-\cos(\Psi_2)\right]\\ &+\frac{\Gamma\left(-\frac{1}{3}\right)}{21.857Z_2}\left[Z_1^{4/3}\cos\left(\frac{4\Psi_1}{3}-\Psi_2\right)-\cos(\Psi_2)\right]\\ &-\frac{\Gamma\left(-\frac{1}{4}\right)}{0.44Z_2}\left[Z_1^{5/4}\cos\left(\frac{5\Psi_1}{4}-\Psi_2\right)-\cos(\Psi_2)\right]\},\end{aligned} \tag{10}$$

where $\Gamma(.)$ is the gamma function, ${}_pF_q(.)$ is the hypergeometric function, $Q_l = \Lambda_1 L\kappa_H^2/k$, and $Z_1$ and $Z_2$ are

$$Z_1 = \frac{1}{3}\sqrt{(3+2Q_l)^2 + Q_H^2(3-2\bar{\Theta}_1)^2}, \tag{11}$$

$$Z_2 = \frac{1}{3}\sqrt{4Q_l^2 + Q_H^2(3-2\bar{\Theta}_1)^2}, \tag{12}$$

where the terms $\Psi_1$ and $\Psi_2$ in Eq. 10 are $\Psi_1 = \arctan\left(\frac{Q_H(3-2\bar{\Theta}_1)}{3+2Q_l}\right)$ and $\Psi_2 = \arctan\left(\frac{Q_H(3-2\bar{\Theta}_1)}{2Q_l}\right)$.

*Proof*: The details for our derivation of the Rytov variance $\sigma_B^2$ for a Gaussian beam wave propagating in Kolmogorov maritime turbulence are given in Supplementary Appendix A.

The derived analytical form of the Rytov variance of the Gaussian beam $\sigma_B^2$ for maritime turbulence in Eq. 10 is different from that of atmospheric turbulence that is derived in the study by Andrews and Phillips (2005). Since the turbulence power spectrum, Rytov variances of plane and Gaussian beam waves, and scintillation index present different forms in the maritime turbulent environment, the performance of maritime FSO links mainly differs from that of conventional FSO links in terms of the turbulence effect.

## 2.3 Pointing error

We use the Beckmann distribution for the pointing error model that is given by Simon and Alouini (2005).

$$f_r(r) = \frac{r}{2\pi\sigma_x\sigma_y}\int_0^{2\pi}\exp\left[-\frac{(r\cos(\varphi)-\mu_x)^2}{2\sigma_x^2} - \frac{\left(r\cos(\varphi)-\mu_y\right)^2}{2\sigma_y^2}\right]d\varphi, \tag{13}$$

where $r \geq 0$, $r = \sqrt{x^2+y^2}$, and $x$ and $y$ are the misalignments in horizontal and vertical directions and independent Gaussian random variables having parameters ($\mu_x$, $\sigma_x$) and ($\mu_y$, $\sigma_y$), respectively. It is well known that the PDF of the pointing error given in Eq. 13 is approximately modeled by Boluda-Ruiz et al. (2016) as

$$f_{h_{pl}}(h_{pl}) = \frac{\varphi_{mod}^2}{(A_0G)^{\varphi_{mod}^2}}h_{pl}^{\varphi_{mod}^2-1}, 0 \leq h_{pl} \leq A_0G, \tag{14}$$

where $\varphi_{mod} = \omega_e/2\sigma_{mod}$, $\omega_e = \omega_b\sqrt{\sqrt{\pi}\mathrm{erf}(\upsilon)/(2\upsilon e^{-\upsilon^2})}$, $\omega_b$ is the beam waist, erf (.) is the error function, $\upsilon = \sqrt{\pi/2}r_a/\omega_b$, $r_a = D_G/2$ is the receiver aperture radius, and $A_0 = \mathrm{erf}^2(\upsilon)$. The parameters $\sigma_{mod}^2$ and $G$ in Eq. 14 are expressed by Boluda-Ruiz et al. (2016) as

$$\sigma_{mod}^2 = \sqrt[3]{\frac{3\mu_x^2\sigma_x^4 + 3\mu_y^2\sigma_y^4 + \sigma_x^6 + \sigma_y^6}{2}}, \tag{15}$$

$$G = \exp\left(\frac{1}{\varphi_{mod}^2} - \frac{1}{2\varphi_x^2} - \frac{1}{2\varphi_y^2} - \frac{\mu_x^2}{2\sigma_x^2\varphi_x^2} - \frac{\mu_y^2}{2\sigma_y^2\varphi_y^2}\right). \tag{16}$$

## 2.4 Angle-of-arrival fluctuations

Assuming that the deviation angle remains in the field of view (FOV) ($\theta_d \leq \theta_{FOV}$), the channel state for AOA fluctuations is found to be (Born and Wolf, 2013)

$$h_{af} = 1 - [J_0(\pi r_a/\lambda)]^2 - [J_1(\pi r_a/\lambda)]^2, \tag{17}$$

where $J_n(.)$ is the $n^{th}$ order Bessel function of the first. To model AOA fluctuations, the PDF of the random variable $\theta_d$ is chosen to be Rayleigh distributed, and it is defined as (Safi et al., 2020)

$$f_{\theta_d}(\theta_d) = \frac{\theta_d}{\sigma_0^2}\exp\left(-\frac{\theta_d^2}{2\sigma_0^2}\right), \theta_d \geq 0, \tag{18}$$

where $\sigma_0^2$ is the variance of $\theta_d$.

# 3 Outage probability analysis

Proposition 2: In Eq. 1, designating $h_{ag} = h_{al}h_{at}h_{pl}$, the conditioned PDF on $\theta_d$ can be found by

$$f_{h_{ag}|\theta_d}(h_{ag}) = \int_{\frac{h_{ag}}{A_0Gh_{al}}}^{\infty}\frac{1}{h_{al}h_{at}}f_{h_{pl}|\theta_d}\left(\frac{h_{ag}}{h_{al}h_{at}}\right)f_{h_{at}}(h_{at})dh_{at}, \tag{19}$$

where $f_{h_{pl}|\theta_d}(.)$ is the conditioned PDF of the misalignments on $\theta_d$ that is obtained as

$$f_{h_{pl}|\theta_d}(h_{pl}) = \frac{\varphi_{mod}^2}{(A_0G)^{\varphi_{mod}^2}} h_{pl}^{\varphi_{mod}^2-1}\cos(\theta_d). \tag{20}$$

Inserting Eqs 5, 20, and expanding the exponential term in Eq. 5, the conditioned PDF becomes

$$f_{h_{ag}|\theta_d}(h_{ag}) = \frac{\varphi_{mod}^2\cos(\theta_d)h_{ag}^{\varphi_{mod}^2-1}\exp(-\sigma_l^2/8)}{(A_0Gh_{al})^{\varphi_{mod}^2}\sqrt{2\pi\sigma_l^2}} \int_{\frac{h_{ag}}{A_0Gh_{al}}}^{\infty} \frac{1}{h_{at}^{\varphi_{mod}^2+3/2}} \exp\left[-\frac{\ln^2(h_{at})}{2\sigma_l^2}\right] dh_{at}. \tag{21}$$

Following the procedures given in Eqs B.1, B.2 in Supplementary Appendix B, the conditioned probability can be written as

$$f_{h_{ag}|\theta_d}(h_{ag}) = \frac{\varphi_{mod}^2\cos(\theta_d)h_{ag}^{\varphi_{mod}^2-1}\exp(-\sigma_l^2/8)}{2(A_0Gh_{al})^{\varphi_{mod}^2}} \exp\left[\frac{\sigma_l^2(\varphi_{mod}^2+1/2)^2}{2}\right][1-\mathrm{erf}(\Upsilon_2)], \tag{22}$$

where $\Upsilon_2 = \frac{\sqrt{2\sigma_l^2}(\varphi_{mod}^2+1/2)}{2} + \frac{1}{\sqrt{2\sigma_l^2}}\ln\left(\frac{h_{ag}}{A_0Gh_{al}}\right)$.

Proof: See Supplementary Appendix B.

Proposition 3: The PDF of the channel can then be calculated as

$$f_h(h) = \int_0^{\infty} h_{af} f_{h_{ag}|\theta_d}(h) f_{\theta_d}(\theta_d) d\theta_d. \tag{23}$$

After applying Eqs C.1, C.2 given in Supplementary Appendix C, the channel PDF reduces to

$$f_h(h) = \frac{h_{af}\varphi_{mod}^2 h^{\varphi_{mod}^2-1}\exp(-\sigma_l^2/8)}{2(A_0Gh_{al})^{\varphi_{mod}^2}} \exp(-\sigma_0^2/2)\,{}_1F_1(-1/2,1/2;\sigma_0^2/2) \times \exp\left[\frac{\sigma_l^2(\varphi_{mod}^2+1/2)^2}{2}\right][1-\mathrm{erf}(\Upsilon_3)], \tag{24}$$

where $\Upsilon_3 = \frac{\sqrt{2\sigma_l^2}(\varphi_{mod}^2+1/2)}{2} + \frac{1}{\sqrt{2\sigma_l^2}}\ln\left(\frac{h}{A_0Gh_{al}}\right)$.

Proof: See Supplementary Appendix C.

Proposition 3: The CDF of the channel can now be expressed by

$$F_h(h) = \int_0^{h} f_h(x)dx. \tag{25}$$

Applying Eqs D.1–D.5 to Eq. 25, the channel CDF can be finally written as

$$\begin{aligned} F_h(h) = {} & \frac{h_{af}\exp(-\sigma_l^2/8)}{2(A_0Gh_{al})^{\varphi_{mod}^2}} \exp\left[\frac{\sigma_l^2(\varphi_{mod}^2+1/2)^2}{2}\right] \exp(-\sigma_0^2/2)\,{}_1F_1\left(-\frac{1}{2},\frac{1}{2};\frac{\sigma_0^2}{2}\right) \\ & \times\left(h^{\varphi_{mod}^2} - (A_0Gh_{al})^{\varphi_{mod}^2}\exp[-\sigma_l^2\varphi_{mod}^2(\varphi_{mod}^2+1/2)]\right. \\ & \times\left\{-\exp\left(\frac{\sigma_l^2\varphi_{mod}^4}{2}\right)\mathrm{erfc}\left(\frac{\sqrt{2\sigma_l^2}\,\varphi_{mod}^2}{2}\right)\right. \\ & +\exp\left(\frac{\sigma_l^2\varphi_{mod}^4}{2}\right)\mathrm{erf}\left(-\frac{\sqrt{2\sigma_l^2}}{4}-\frac{1}{\sqrt{2\sigma_l^2}}\Upsilon_4\right) - \exp\left(\frac{\sigma_l^2\varphi_{mod}^4}{2}\right) \\ & \times\mathrm{erf}\left(\frac{\sqrt{2\sigma_l^2}\,\varphi_{mod}^2}{2}\right) + \exp[\sigma_l^2\varphi_{mod}^2(\varphi_{mod}^2+1/2)+\varphi_{mod}^2\Upsilon_4] \\ & \left.\left.\times\mathrm{erf}\left(\frac{\sqrt{2\sigma_l^2}\,(\varphi_{mod}^2+1/2)}{2}+\frac{1}{\sqrt{2\sigma_l^2}}\Upsilon_4\right)\right\}\right), \end{aligned} \tag{26}$$

where $\Upsilon_4 = \ln\left(\frac{h}{A_0Gh_{al}}\right)$.

Proof: See Supplementary Appendix D.

**TABLE 1** Chosen parameters.

| Symbol | Description | Value |
|---|---|---|
| $\lambda$ | Wavelength | 1,550 nm |
| $h_{th}$ | Channel threshold | $10^{-4}$ |
| $L$ | Link length | 3 km |
| $C_n^2$ | Turbulence structure constant | $5\times10^{-16}$ m$^2$/s$^3$ |
| $V$ | Visibility | 10 km |
| $D_G$ | Receiver aperture diameter | 2 cm |
| $r_a$ | Receiver aperture radius | $r_a = D_G/2$ |
| $W_0$ | Gaussian beam radius | 2 cm |
| $F_0$ | Phase front radius of curvature (collimated beam) | $\infty$ |
| $\sigma_0$ | Orientation deviation | 15 mrad |
| $\omega_b$ | Beam waist | $10\times r_a$ |
| $\sigma_x^2$ | Displacement variance in the horizontal axis | $\sigma_x = 2\times r_a$ |
| $\sigma_y^2$ | Displacement variance in the vertical axis | $\sigma_y = 2\times r_a$ |
| $\mu_x$ | Boresight pointing error in the horizontal axis | $\mu_x = 1\times r_a$ |
| $\mu_y$ | Boresight pointing error in the vertical axis | $\mu_y = 2\times r_a$ |
| $l_0$ | Inner scale length | 1 mm |
| $L_0$ | Outer scale length | 50 m |

The outage probability is essentially the CDF evaluated at the predetermined threshold $h_{th}$, i.e.,

$$P_{out} = P_r(h \le h_{th}) = F_h(h_{th}), \tag{27}$$

where $h_{th}$ is the threshold level for the combined channel state.

Finally, the outage probability for a maritime FSO communication system can be written as

$$\begin{aligned} P_{out} = {} & \frac{h_{af}\exp(-\sigma_l^2/8)}{2(A_0Gh_{al})^{\varphi_{mod}^2}} \exp\left[\frac{\sigma_l^2(\varphi_{mod}^2+1/2)^2}{2}\right] \exp(-\sigma_0^2/2)\,{}_1F_1\left(-\frac{1}{2},\frac{1}{2};\frac{\sigma_0^2}{2}\right) \\ & \times\left(h_{th}^{\varphi_{mod}^2} - (A_0Gh_{al})^{\varphi_{mod}^2}\exp[-\sigma_l^2\varphi_{mod}^2(\varphi_{mod}^2+1/2)]\right. \\ & \times\left\{-\exp\left(\frac{\sigma_l^2\varphi_{mod}^4}{2}\right)\mathrm{erfc}\left(\frac{\sqrt{2\sigma_l^2}\,\varphi_{mod}^2}{2}\right)\right. + \exp\left(\frac{\sigma_l^2\varphi_{mod}^4}{2}\right) \\ & \times\mathrm{erf}\left(-\frac{\sqrt{2\sigma_l^2}}{4}-\frac{1}{\sqrt{2\sigma_l^2}}\Upsilon_5\right) \\ & -\exp\left(\frac{\sigma_l^2\varphi_{mod}^4}{2}\right)\mathrm{erf}\left(\frac{\sqrt{2\sigma_l^2}\,\varphi_{mod}^2}{2}\right) + \exp[\sigma_l^2\varphi_{mod}^2(\varphi_{mod}^2+1/2)+\varphi_{mod}^2\Upsilon_5] \\ & \left.\left.\times\mathrm{erf}\left(\frac{\sqrt{2\sigma_l^2}\,(\varphi_{mod}^2+1/2)}{2}+\frac{1}{\sqrt{2\sigma_l^2}}\Upsilon_5\right)\right\}\right), \end{aligned} \tag{28}$$

where $\Upsilon_5 = \ln\left(\frac{h_{th}}{A_0Gh_{al}}\right)$. Equation 28 is in analytical form; uses the combination of exponential, error, and natural logarithm functions; and reflects the performance of an FSO system operating in the maritime environment without involving any complex operation, e.g., integration. The influence of maritime turbulence, pointing error, AOA fluctuations, and attenuation is embedded in Eq. 28, and this yields a comprehensive exploration possibility for the performance of FSO links.

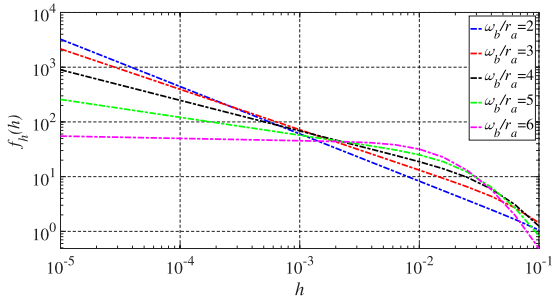


FIGURE 2
Channel PDF variation as a function of the channel state for different values of the beam waist.

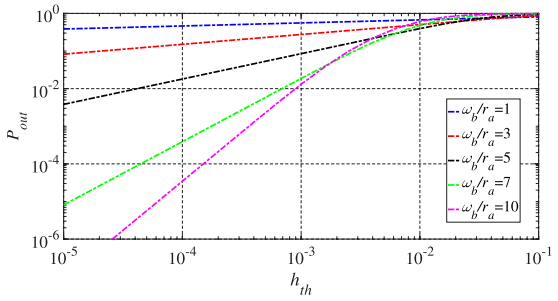


FIGURE 5
Outage probability variation versus the channel state threshold for different values of beam waists.

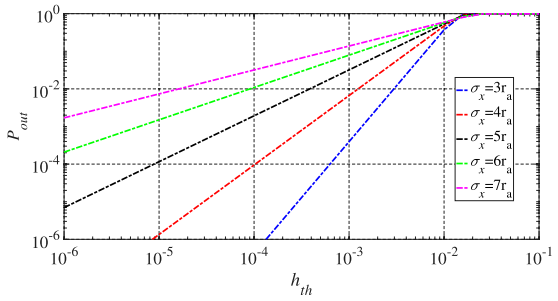


FIGURE 3
Outage probability variation versus the channel state threshold for different values of horizontal displacement.

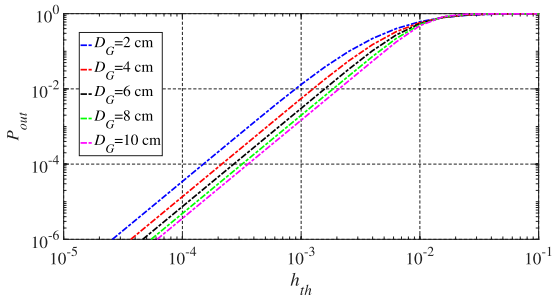


FIGURE 6
Outage probability variation versus the channel state threshold for different values of the receiver aperture.

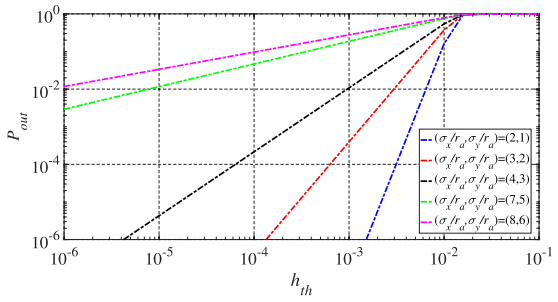


FIGURE 4
Outage probability variation versus the channel state threshold for different values of both horizontal and elevation displacements.

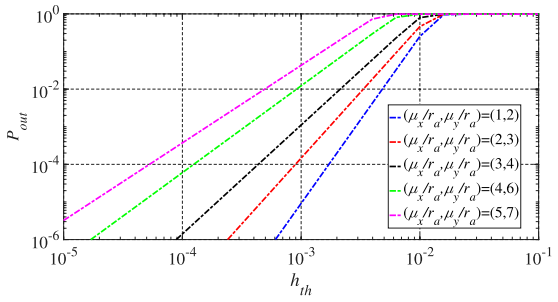


FIGURE 7
Outage probability variation versus the channel state threshold for different values of the boresight error values.

## 4 Results and discussion

In this section, the outage performance of a maritime FSO communication system is presented depending on various parameters. All results are obtained by adopting the fixed parameter values (that can be encountered in practical communication links) given in Table 1, and parameter values different from those given in Table 1 are given either in figures or in figure captions.

In Figure 2, the PDF of the channel is plotted versus the channel state for different values of the beam waist. It is seen from Figure 2 that the channel distribution tends to decrease with the increase of channel state in general. It is also observed from Figure 2 that channel PDF stands smaller for higher values of beam waist when the channel state is at a low level (e.g., $h \lesssim 10^{-3}$). Then, the channel PDF saturates, and the decreasing trend with the increase of beam waist reverses.

Figure 3 illustrates the outage performance of a maritime FSO communication system as a function of channel threshold for various values of horizontal displacement. We observe from the figure that the outage probability monotonically increases, hence the performance of the FSO communication system degrades, together with the rise of channel state threshold $h_{th}$. For example, keeping horizontal beam displacement as $\sigma_x = 5 \times r_a$, the outage probability increases from $P_{out} \sim 7 \times 10^{-6}$ to $P_{out} \sim 5.3 \times 10^{-1}$ when the channel state threshold increases from $h_{th} = 10^{-6}$ to $h_{th} = 10^{-2}$. The performance degradation with the increase of channel state threshold can also be seen in Figures 4–7.

Since the Beckmann distribution permits modeling asymmetric beam displacement, it is also aimed to reflect the performance of the maritime FSO communication system when beam displacement varies in one direction, as shown in Figure 3. Fixing the channel state threshold at $h_{th} = 10^{-3}$, the outage probability takes the values of $P_{out} \sim 3.9 \times 10^{-4}$, $P_{out} \sim 3.2 \times 10^{-2}$, and $P_{out} \sim 1.4 \times 10^{-1}$ for the values of horizontal beam displacement $\sigma_x/r_a = 3$, $\sigma_x/r_a = 5$, and $\sigma_x/r_a = 7$, respectively, showing the significant performance degradation with the increase of beam displacement even if it is in one direction. Moreover, the outage probability variation with the beam displacement taking place in two directions is shown in Figure 4. It is seen that increasing the beam displacement in both horizontal and vertical directions causes a significant increase in the outage probability. For example, changing $(\sigma_x/r_a, \sigma_y/r_a) = (4, 3)$ to $(\sigma_x/r_a, \sigma_y/r_a) = (8, 6)$ causes a raise in the outage probability from $P_{out} \sim 2.1 \times 10^{-4}$ to $P_{out} \sim 9.6 \times 10^{-2}$, while the channel state threshold is fixed at $h_{th} = 10^{-4}$. It is also observed that the outage probability of two-dimensional beam displacements remains higher than that of one-dimensional displacement. Since the receiver aperture radius usually remains on the order of several centimeters, it is evident that the beam displacement of tens of centimeters or more will seriously degrade the performance of maritime FSO communication systems.

The dependence of outage probability on the beam waist is shown in Figure 5. It is noteworthy to mention that a maritime FSO communication system benefits from the higher beam waist, which may be the result of the increasing possibility of the optical beam being picked up by the photodetector. When the channel state threshold is $h_{th} = 10^{-3}$, the outage probability sharply falls from $P_{out} \sim 4.6 \times 10^{-1}$ to $P_{out} \sim 3.4 \times 10^{-5}$, with the increase of the beam waist increasing from $\omega_b/r_a = 1$ to $\omega_b/r_a = 10$. It is also seen that the decrease in the outage probability with the increase of the beam waist breaks down after a certain level of channel state threshold (e.g., $h_{th} \gtrsim 10^{-2}$). This shows that maritime FSO communication systems can benefit from beam waists up to a certain level. However, if the beam waist exceeds this certain level, the performance-degrading effect is observed. This variation clearly illustrates that maintaining the optimum level of beam waist will yield a performance-improving impact.

The benefit of aperture averaging, one of the most effective methods used to mitigate the turbulence effect, is illustrated in Figure 6. From Figure 6, we observe that using larger aperture size at the receiver improves the performance of the maritime FSO communication system. Outage probability decreases from $P_{out} \sim 1.3 \times 10^{-2}$ to $P_{out} \sim 1.5 \times 10^{-3}$ with the increase of receiver aperture diameter from $D_G = 2$ cm to $D_G = 10$ cm. We again note that the benefit of aperture averaging maintains up to a certain level of channel state threshold ($h_{th} \sim 10^{-2}$). In general, it can be stated that the performance-impairing impact of maritime turbulence-induced phenomena, such as intensity fluctuations, beam spread, and beam waist, can be reversed by increasing the receiver aperture size.

Figure 7 reveals how boresight error affects the performance of the maritime FSO communication system. We find from Figure 7 that the impact of boresight error on the FSO communication system can be substantial. This can be verified by varying the boresight errors in both horizontal and vertical directions as ($\mu_x$/

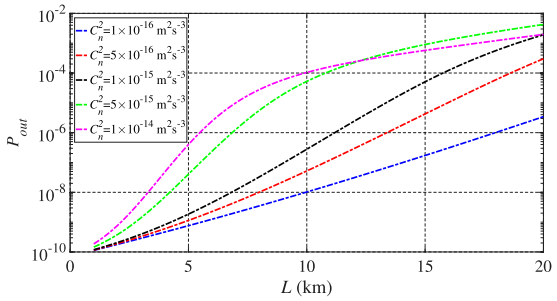


FIGURE 8
Outage probability variation versus the link length for different values of the turbulence structure constant.

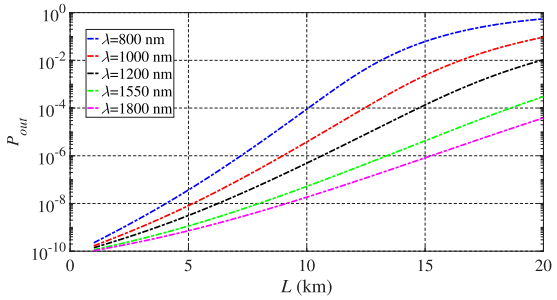


FIGURE 9
Outage probability variation versus the link length for different values of the wavelength.

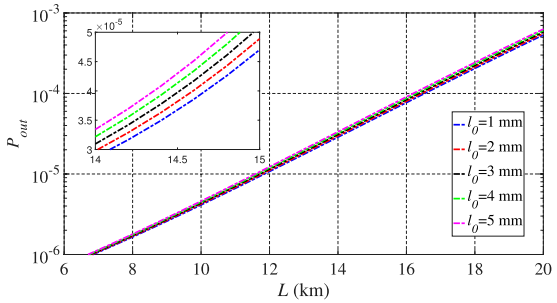


FIGURE 10
Outage probability variation versus the link length for different values of the turbulence inner scale.

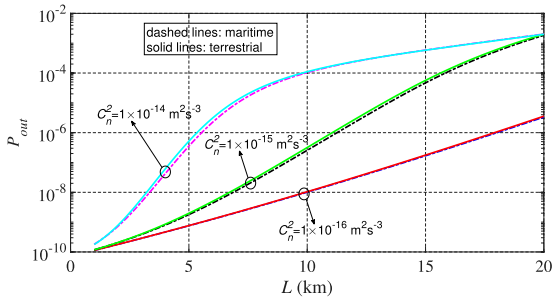


FIGURE 11
Comparison of the outage probability of both maritime and terrestrial links versus the propagation distance for different values of the turbulence structure constant.

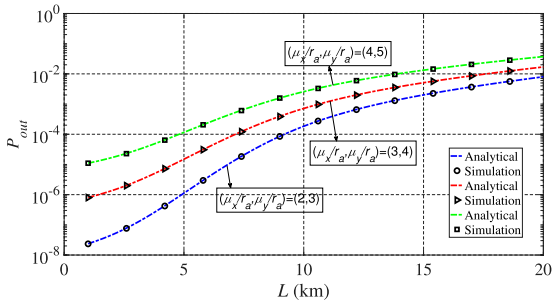


FIGURE 14
Analytical and simulated outage probabilities of the maritime FSO link versus the propagation distance for different values of the boresight error values.

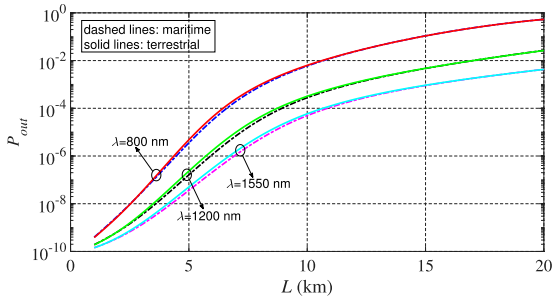


FIGURE 12
Comparison of the outage probability of both the maritime and terrestrial links versus the propagation distance for different values of the wavelength.

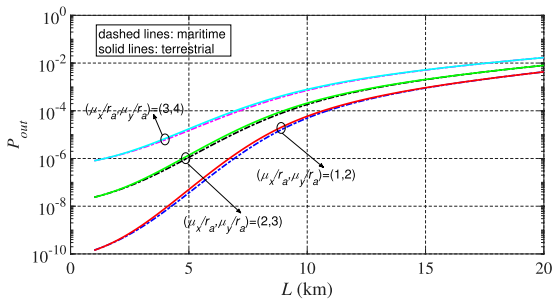


FIGURE 13
Comparison of the outage probability of both the maritime and terrestrial links versus the propagation distance for different values of the boresight error values.

$r_a, \mu_y/r_a) = (1, 2)$, $(\mu_x/r_a, \mu_y/r_a) = (3, 4)$, and $(\mu_x/r_a, \mu_y/r_a) = (5, 7)$ that yield the outage probability as $P_{out} \sim 9.1 \times 10^{-6}$, $P_{out} \sim 1.1 \times 10^{-3}$, and $P_{out} \sim 4.3 \times 10^{-2}$, respectively, for the channel state threshold $h_{th} = 10^{-3}$.

In Figure 8, the variation of outage performance is illustrated versus the link length for various values of the turbulence structure constant. As expected, in Figures 9–13, the outage performance reduces with the increase of the link length, while outage probability takes its smallest value at the closest distance $L = 1$ km. It is also seen from Figure 8 that maritime turbulence causes a remarkable performance degradation by yielding a higher outage probability for higher values of the turbulence constant. Increasing the turbulence structure constant from $C_n^2 = 1 \times 10^{-16}$ m$^2$/s$^3$ to $C_n^2 = 1 \times 10^{-14}$ m$^2$/s$^3$ produces a change in the outage probability from $P_{out} \sim 2.1 \times 10^{-9}$ to $P_{out} \sim 1 \times 10^{-5}$ at link length $L = 7$ km. Another important conclusion from Figure 8 is that the outage probability becomes smaller for higher turbulence levels after a certain level of distance that can be seen from the plot for $C_n^2 = 1 \times 10^{-14}$ m$^2$/s$^3$. This is due to the combined effect of higher turbulence and longer distance that puts the optical beam into a saturated turbulent regime. The trend change resulting from the saturation phenomenon in turbulence regimes is expressed by the continuity of irradiance fluctuations due to the small scales. First introduced in Tatarskii's theory, the validity of the saturation phenomenon was experimentally investigated by Clifford et al. (1974), and it was concluded that the reason for this effect is the eddies smaller than the Fresnel zone.

The variation of outage performance depending on the wavelength is given in Figure 9. Being valid in terms of the turbulence effect, the performance of the maritime FSO system improves when the wavelength is kept higher. However, the optimum wavelength should be selected not only by turbulence but also by absorption and scattering effects. In Figure 10, the inner scale length effect on the outage performance is presented. While $l_0 = 5$ mm yields the highest outage probability, the difference between outage probabilities of maritime FSO links with the change of inner scale lengths stands quite small.

Since a part of the maritime-based ship-to-shore link may cover terrestrial propagation, we aim to reflect the behavior of the FSO communication system in terrestrial link and the difference from the maritime FSO for the same parameters. To give a perspective to the readers, we plot the comparison of the outage performances of maritime and terrestrial FSO links versus the link length for different values of the turbulence structure constant, wavelength, and boresight errors in Figures 11–13, respectively. All parameters are set to the same values for both maritime and terrestrial links. The scintillation index for the terrestrial link is calculated by Rytov variances of plane and Gaussian beam waves propagating in the

atmospheric turbulence medium. The Rytov variances of the plane wave $\sigma_{R_T}^2$ and Gaussian beam wave $\sigma_{B_T}^2$ in the terrestrial turbulent medium are found in an analytical form (Andrews and Phillips, 2005) as

$$\sigma_{R_T}^2 = 1.23 C_n^2 k^{7/6} L^{11/6}, \tag{29}$$

$$\sigma_{B_T}^2 = 3.86 \sigma_{R_T}^2 \mathrm{Re}\left[ i^{\frac{5}{6}} {}_2F_1\left( -\frac{5}{6}, \frac{11}{6}; \frac{17}{6}; \bar{\Theta}_1 + i\Lambda_1 \right) - \frac{11}{6} \Lambda_1^{\frac{5}{6}} \right]. \tag{30}$$

The comparison of the performances of FSO links is made by using the Rytov variances of plane wave and Gaussian beam wave of the mediums themselves in the scintillation index calculation, i.e., Eqs 9, 10 for the maritime link and Eqs 29, 30 for the terrestrial link. As can be seen from all three figures, although the performance of the maritime FSO communication system remains slightly better than that of the terrestrial FSO communication system, we can say that the performances of both systems are very close to each other over the whole range of interest. Again, the performance degradation effect of higher turbulence structure constant, smaller Gaussian beam wavelength, and higher boresight error is observed from Figures 11–13, respectively, for both terrestrial and maritime FSO communication links.

Finally, to validate our analytical results with simulation, we present the outage performance of the maritime FSO link versus the link length for various boresight error values in Figure 14. For different values of boresight error, it is seen that analytical and simulation results are in good agreement, which shows the correctness of our analysis.

## 5 Conclusion

This study investigates the outage performance of the maritime FSO communication system. The effects of atmospheric turbulence, pointing error, AOA fluctuations, and attenuation are taken into account. The results show that maritime turbulence and pointing error remain the main factors in terms of reducing the performance of FSO communication systems. The maritime turbulent channel is modeled by a lognormal distribution, and it is examined in a wide range. To calculate the scintillation index in the maritime turbulent environment, a new closed-form expression of the Rytov variance for the Gaussian beam is obtained for a Kolmogorov turbulent spectrum. The impacts of beam displacement and boresight error in both horizontal and vertical directions are revealed by using the approximated Beckmann distribution. New closed-form expressions for channel PDF, CDF, and outage probability are also derived. It is shown that the performances of maritime and terrestrial FSO communication systems are very close to each other for the same parameters.

## Data availability statement

The original contributions presented in the study are included in the article/Supplementary Material, further inquiries can be directed to the corresponding author.

## Author contributions

All authors listed have made a substantial, direct, and intellectual contribution to the work and approved it for publication.

## Conflict of interest

The authors declare that the research was conducted in the absence of any commercial or financial relationships that could be construed as a potential conflict of interest.

## Publisher's note

All claims expressed in this article are solely those of the authors and do not necessarily represent those of their affiliated organizations, or those of the publisher, the editors, and the reviewers. Any product that may be evaluated in this article, or claim that may be made by its manufacturer, is not guaranteed or endorsed by the publisher.

## Supplementary material

The Supplementary Material for this article can be found online at: https://www.frontiersin.org/articles/10.3389/frcmn.2023.1184911/full#supplementary-material

## References


Alqurashi, F. S., Trichili, A., Saeed, N., Ooi, B., and Alouini, M. S. (2022). Maritime communications: A survey on enabling technologies, opportunities, and challenges. arXiv preprint arXiv:2204.12824.

Andrews, L. C., and Phillips, R. L. (2005). *Laser beam propagation through random media*. Bellingham: SPIE.

Awan, M. S., Leitgeb, E., Muhammad, S. S., Nadeem, F., Khan, M. S., Capsoni, C., et al. (2008). "Distribution function for continental and maritime fog environments for optical wireless communication," in 2008 6th International Symposium on Communication Systems, Networks and Digital Signal Processing, Graz, Austria, 25-25 July 2008 (IEEE), 260–264.

Boluda-Ruiz, R., García-Zambrana, A., Castillo-Vázquez, C., and Castillo-Vázquez, B. (2016). Novel approximation of misalignment fading modeled by beckmann distribution on free-space optical links. *Opt. Express* 24, 22635–22649. doi:10.1364/oe.24.022635

Born, M., and Wolf, E. (2013). *Principles of optics: Electromagnetic theory of propagation, interference and diffraction of light*. Cambridge, U.K: Cambridge Univ. Press.

Cheng, M., Guo, L., and Zhang, Y. (2015). Scintillation and aperture averaging for Gaussian beams through non-Kolmogorov maritime atmospheric turbulence channels. *Opt. Express* 23, 32606–32621. doi:10.1364/oe.23.032606

Clifford, S. F., Ochs, G. R., and Lawrence, R. S. (1974). Saturation of optical scintillation by strong turbulence. *JOSA* 64, 148–154. doi:10.1364/josa.64.000148

Cvijetic, M., and Li, M. (2017). "Characterization of free space optical channels for terrestrial and maritime air conditions," in 2017 19th International Conference on Transparent Optical Networks (ICTON), Girona, Spain, 02-06 July 2017 (IEEE), 1–5.

Gadwal, V., and Hammel, S. (2006). Free-space optical communication links in a marine environment. *Free-Space Laser Commun. VI* 6304, 161–171.

Gradshteyn, I. S., and Ryzhik, I. M. (2014). *Table of integrals, series, and products*. Academic Press.

Grayshan, K. J., Vetelino, F. S., and Young, C. Y. (2008). A marine atmospheric spectrum for laser propagation. *Waves Random Complex Media* 18, 173–184. doi:10.1080/17455030701541154

Gregory, M., and Badri-Hoeher, S. (2011). "Characterization of maritime rf/fso channel," in 2011 International conference on space optical systems and applications (ICSOS), Santa Monica, CA, USA, 11-13 May 2011 (IEEE), 21–27.

Guan, S., Wang, J., Jiang, C., Duan, R., Ren, Y., and Quek, T. Q. S. (2021). Magicnet: The maritime giant cellular network. *IEEE Commun. Mag.* 59, 117–123. doi:10.1109/mcom.001.2000831

Jo, S. W., and Shim, W. S. (2019). LTE-maritime: High-speed maritime wireless communication based on LTE technology. *IEEE Access* 7, 53172–53181. doi:10.1109/access.2019.2912392

Juarez, J. C., Sluz, J. E., Nelson, C., Airola, M. B., Fitch, M. J., Young, D. W., et al. (2010). Free-space optical channel characterization in the maritime environment. *Atmos. Propag.* 7685, 129–136. doi:10.1364/OE.26.006614

Kampouraki, M. N., Stasinakis, A. N., Nistazakis, H. E., Tsigopoulos, A. D., Tombras, G. S., Chronopoulos, G. G., et al. (2014). "Experimental and theoretical bit rate estimation of turbulent fso link over the maritime area at piraeus port," in *Proceedings of the 6th international conference from scientific computing to computational engineering* (Athens, Greece: Spinger), 9–12.

Kidston, D., and Kunz, T. (2008). Challenges and opportunities in managing maritime networks. *IEEE Commun. Mag.* 46, 162–168. doi:10.1109/mcom.2008.4644135

Kim, H. J., Tiwari, S. V., and Chung, Y. H. (2016). Multi-hop relay-based maritime visible light communication. *Chin. Opt. Lett.* 14, 050607. doi:10.3788/col201614.050607

Lionis, A., Peppas, K., Nistazakis, H. E., Tsigopoulos, A. D., and Cohn, K. (2020). Experimental performance analysis of an optical communication channel over maritime environment. *Electronics* 9, 1109. doi:10.3390/electronics9071109

Naboulsi, M. C. A., Sizun, H., and de Fornel, F. (2004). Fog attenuation prediction for optical and infrared waves. *Opt. Eng.* 43, 319–329. doi:10.1117/1.1637611

Qiao, Y. Z., Lu, Z. H., Yan, B. L., Li, C. J., Zhang, H., Lin, W., et al. (2021). Performance of differential phase shift keying maritime laser communication over log-normal distribution turbulence channel. *Optoelectron. Lett.* 17, 90–95. doi:10.1007/s11801-021-9211-9

Rabinovich, W. S., Mahon, R., Gilbreath, G. C., Goetz, P. G., and Moore, C. I. (2005). Free-space optical communications link at 1550 nm using multiple-quantum-well modulating retroreflectors in a marine environment. *Opt. Eng.* 44, 056001. doi:10.1117/1.1906230

Safi, H., Dargahi, A., Cheng, J., and Safari, M. (2020). Analytical channel model and link design optimization for ground-to-hap free-space optical communications. *J. Light. Technol.* 38, 5036–5047. doi:10.1109/jlt.2020.2997806

Simon, M. K., and Alouini, M. S. (2005). *Digital communication over fading channels*. New Jersey: John Wiley & Sons Inc.

Sluz, J. E., Juarez, J. C., Sova, R. M., Young, D. W., and Nelson, C. (2010). "Characterization of data transmission through a maritime free-space optical channel with a custom bit error rate tester," in *Enabling photonics technologies for defense, security, and aerospace applications VI* (Orlando, Florida, United States: SPIE), 69–79.

Wolfram Inc (2023b). *The wolfram functions site*. Oxford, UK: WolframAlpha LLC

Wolfram Inc (2023a). *Wolfram alpha*. Oxford, UK: WolframAlpha LLC.

Yang, T., and Shen, X. S. (2014). *Maritime wideband communication networks: Video transmission scheduling*. Springer.

Zolich, A., Palma, D., Kansanen, K., Fjørtoft, K., Sousa, J., Johansson, K. H., et al. (2019). Survey on communication and networks for autonomous marine systems. *J. Intelligent Robotic Syst.* 95, 789–813. doi:10.1007/s10846-018-0833-5